Image System Solution for Store Aerodynamics with Interference—Part I

Fred W. Martin*
Auburn University, Auburn, Ala.

Grady H. Saunders†
ARO, Inc., Arnold Air Force Station, Tenn.

and

Charles J. Smith‡
Electronic Data Systems, New York, N.Y.

The aerodynamic interference problem for external aircraft-stores has been analyzed using the image system technique. In order to facilitate this analysis it has been assumed that small perturbation solutions are valid. It is further assumed that the external stores are slender, axisymmetric bodies and that the interference can be analyzed by first assuming a cross-flow solution. Both body-body and wing-body interference solutions have been obtained. The latter are covered in a later extension to this paper. For the body-body solution, the image systems in the cross-flow plane consist of source-sink pairs appropriately located by using the Milne-Thomson circle theorem. The actual three-dimensional source-sink pairs are displaced from the body axis according to the cross-flow image system. The strengths of the source-sink pairs are then determined by the Rankine method. Good agreement has been found between the theoretical and experimental results. It is felt that this approach to the interference problem is a significant advancement in that this technique requires only successive superposition whereas most other methods such as vortex lattice, source panels, etc., require, in general, simultaneous solutions.

Nomenclature

a_{ij}, b_{ij}, d_{ij} = coefficients defined by Eqs. (25-27)
$a'_{ij}, b'_{ij}, d'_{ij}$ = coefficients formed from Eqs. (25-27)
C_{ij} = coefficient defined by Eq. (12)
e = coefficients of z_i
f = coefficients of z_i
i = $(-1)^{1/2}$
m, m_i = strength of three-dimensional source (single body)
m_i' = strength of added source and sink
M = Mach number
N = number of sources, equations, etc.
r = radius of body (Fig. 6)
r_i = radius of body at i^{th} source point
r_j = radius to j^{th} point in flowfield at x_j location
u_x = axial perturbation velocity component
u_r, u_θ = radial and angular perturbation velocity components
U_∞ = freestream velocity
x, y = body axes, first body
x_i, x_j = axial distances from nose of body to i^{th} and j^{th} point
x_o, y_o = distances between body center lines
x', y' = body axes, second body
z_i = nondimensional source strength/velocity parameter defined by Eq. (7)
Z, Z' = coefficients defined by Eqs. (28-30)
δ, δ_i = source displacement distances (Figs. 1 and 4)
θ = angle shown in Fig. 4
ϕ_j = total perturbation velocity potential
ρ_{ij} = distance from i^{th} source to j^{th} point (Fig. 3)
ρ_{ijl}, ρ_{ij2} = distance from displaced source point to point j in flowfield (Fig. 4)
ρ'_{ijl}, ρ'_{ij2} = distances from body center line to point j in flowfield (Fig. 4)
= property of image system (unprimed property with same symbol is property of single body system)
$[\ ]$ = square matrix
$\{\ \}$ = column matrix
$[\ ]^{-1}$ = matrix inverse

Received January 15, 1974; revision received October 18, 1974.
Index categories: Aircraft Aerodynamics (Including Component Aerodynamics; Subsonic and Transonic Flow.

*Professor, Aerospace Engineering Department, Member AIAA.
†Engineer; formerly Graduate Student, Aerospace Engineering Department, Auburn University, Auburn, Ala.
‡Systems Engineer; formerly Graduate Student, Aerospace Engineering Department, Auburn University, Auburn, Ala.

Introduction

THIS paper, which consists of two parts, concerns a theoretical approach for the determination of aerodynamic force coefficients in an interference flowfield. In Part I, two-, three-, and four-body cases are analyzed which yield good agreement with experiment. In Part II, wing-body and wing-pylon body problems are analyzed. In this analysis it has been assumed that small perturbation solutions are valid, and thus the governing equation of motion is the familiar Prandtl-Glauert equation.

$$(1-M^2)\phi_{xx}+\phi_{yy}+\phi_{zz}=0 \tag{1}$$

which is subject to the boundary conditions of no fluid flow into the body and vanishing perturbations at large distances from the body. Since the equation is linear, superposition of elementary solutions will allow build-up of a complex flow which satisfies the boundary conditions. The widely used vortex-lattice and line source solutions for planar and axisymmetric flows represent two common examples of the superposition of simple solutions to form more complex flows. However, when systems such as the flowfields for planar wings and axisymmetric bodies are combined it is not possible

to simply superimpose the results for the separate systems. The mutual interference of the flowfields requires that adjustments be made to the elementary source and/or vortex distribution in order to satisfy the body boundary conditions. Numerous examples of this general technique can be found throughout the literature; to name a very few, Woodward, Bradley and Miller,[1,2] and Kalman, Rodden and Giesing.[3] In most of these papers, the solution for an arbitrary wing-body combination is found by representing it with a system of source, doublet, and vortex singularities. Simultaneous solutions are then required for the resulting system of equations.

The technique used in this paper differs from those in Refs. 1-3 in that the solution for the mutual interference is generated using the solutions for the isolated bodies and superimposing an appropriate image system of source and/or vortex singularities. Although this method is limited at this time to geometric shapes for which a reasonable image system is easily obtained, it is particularly useful for the study of external stores which are slender, axisymmetric bodies.

General Theoretical Considerations

The concepts used in this analysis are based on the assumptions generally used in slender body theory. Some departure from the usual crossflow solutions are made, however, which are outlined in the following sections and more fully documented by Smith[4] and Walkley.[5]

Boundary Conditions

Any particular solution of Eq. (1) which is representative of an actual flow must satisfy the boundary conditions at infinity and at the surfaces of any bodies which are present in the flowfield. Since only elementary solutions are required in this development, the boundary condition far from the body will be satisfied. As usual, the body boundary condition is satisfied by setting the component of the velocity normal to the body to zero. For an axisymmetric body, this boundary condition may be expressed mathematically as

$$\frac{dr}{dx} = \frac{u_r/U_\infty}{(1+u_x/U_\infty)} \tag{2}$$

For a single body at zero angle-of-attack, the angular velocity component, u_θ, is identically zero. In the multiple-body case, u_θ is not generally zero, but it does satisfy the tangential flow requirement at all points on an axisymmetric body. Therefore, Eq. (2) is the correct expression for the body boundary condition for the multiple-body case as well as for the isolated body.

Elementary Flow Methods

A two-dimensional cross-flow solution was developed by Martin[6] (Fig. 1) which was subsequently used as a basis for a cross-flow image system that was developed as a possible correction for the three-dimensional interference problem.[7]

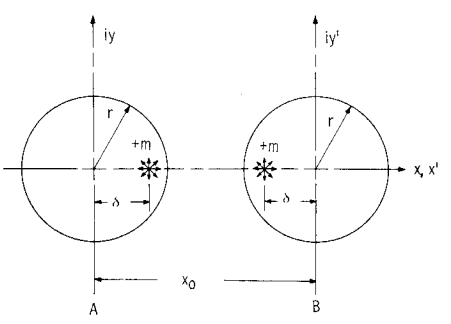

Fig. 1 Two-dimensional cross-flow solution for two similar axisymmetric bodies.

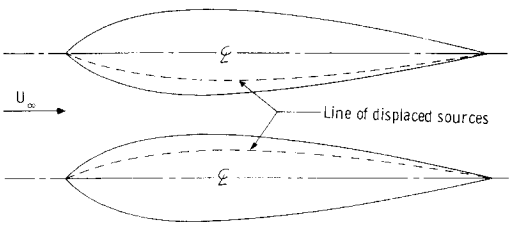

Fig. 2 Schematic of displaced line sources for the cross-flow correction given in Ref. 7.

While this latter analysis did not yield good agreement with experiment, it lead to the development reported by Smith[4] for the two-body case.

In the original work,[7] the author proposed a solution in terms of a continuous distributed line source which was displaced according to the two-dimensional image system (Fig. 2). Generally, it is not possible to find a continuous line source for generating the body and the solution is approximated by a number of finite line sources. This approach leads to geometric complexities, however, because of the curved displacement line (Fig. 2). For this reason, Smith[4] replaced the line sources with a number of three-dimensional point sources and sinks. This also has the advantage of requiring half as many calculations as the solution for the same number of line sources because the integrated effect of a line source at a field point is a function of the distance from each end of the source to the point, whereas the effect of a point source depends only on the distance between the points. Thus, the point sources, rather than line sources, are used throughout this analysis.

For the analysis of the interferences between the wing-pylon-body presented in Part II, a simple horse-shoe vortex has been used in order to generate the wing-pylon flowfield. A vortex image system is then obtained within the axisymmetric body.

In all cases in this study, the solutions for the isolated bodies of revolution are generated by distributing point sources along the body axis. It is assumed, however, that other solution techniques could be applied.

Single-Body Solution

The single, or isolated, body solutions used in this work have been generated using N three-dimensional sources of different strengths, m_i, distributed uniformly along the body center line. The total perturbation velocity potential, ϕ_s, at a point j may be expressed as

$$\phi_j = -\sum_{i=1}^{N} \frac{m_i}{4\pi} \frac{1}{\rho_{ij}} \tag{3}$$

Differentiating Eq. (3) and expressing the results in cylindrical coordinates, the perturbation velocity components at the jth point are

$$u_{x_j} = \sum_{i=1}^{N} \frac{m_i}{4\pi} \frac{\partial}{\partial x_j}\left(\frac{1}{\rho_{ij}}\right) \tag{4}$$

and

$$u_{r_j} = -\sum_{i=1}^{N} \frac{m_i}{4\pi} \frac{\partial}{\partial r_j}\left(\frac{1}{\rho_{ij}}\right) \tag{5}$$

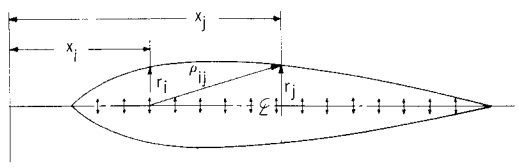

Fig. 3 Geometric relations for the single-body case.

Due to symmetry, u_θ is zero for the case of a single body at zero angle of attack. As can be seen from Fig. 3, ρ_{ij} is not a function of θ and is given by

$$\rho_{ij}=[(x_j-x_i)^2+r_j^2]^{1/2} \tag{6}$$

If a new variable z_i is introduced, defined such that it is proportional to the source strength; i.e.,

$$z_i=m_i/4\pi U_\infty \tag{7}$$

Equations (4) and (5) can be used to form the velocity components in the nondimensional forms,

$$\frac{u_{xj}}{U_\infty}=-\sum_{i=1}^{N} z_i\frac{x_i-x_j}{\rho_{ij}^3} \tag{8}$$

and

$$\frac{u_{rj}}{U_\infty}\sum_{i=1}^{N} z_i\frac{r_j}{\rho_{ij}^3} \tag{9}$$

Equations (8) and (9) can be applied to any nonsingular point in the flowfield to determine the velocity ratios. Referring to Eq. (2), it can be seen that the body boundary condition in terms of the velocity ratios is specified by

$$\frac{dr_j}{dx_j}=\sum_{i=1}^{N} z_i(r_j/\rho_{ij}^3)\Big/1+\sum_{i=1}^{n} z_i[(x_j-x_i)/\rho_{ij}^3] \tag{10}$$

Rearranging this result yields a set of N simultaneous linear equations in the form

$$\sum_{i=1}^{N} z_iC_{ij}=\frac{dr_j}{dx_j}\quad(j=1,2,3,\ldots,n) \tag{11}$$

where the coefficient C_{ij} is expressed by

$$C_{ij}=\frac{(x_j-x_i)(dr_j/dx_j)+r_j}{\rho_{ij}^3} \tag{12}$$

Equation (11) may be written in the equivalent matrix form

$$[C]\{Z\}=\left\{\frac{dr}{dx}\right\} \tag{13}$$

which can be solved by matrix inversion to give

$$\{Z\}=[C]^{-1}\left\{\frac{dr}{dx}\right\} \tag{14}$$

The array of source strengths as calculated by this method satisfies the body boundary condition for any isolated axisymmetric body at zero angle of attack.

Two-Body Solution

Consider the case of two identical axisymmetric bodies aligned such that one is directly above the other. At any axial station the cross-flow image system when combined with the original source for the two-dimensional case gives a system which is the equivalent to displacing each source toward its corresponding source in the other body, as shown in Fig. 1. The distances which the sources are displaced are derived from repeated applications of the Milne-Thomson circle theorem (Ref. 6) and are given by:

$$\delta_i=\frac{y_o}{2}\left\{1-\left(1-\left(\frac{2r_i}{yo}\right)^2\right)^{1/2}\right\} \tag{15}$$

Since the bodies are identical and aligned in the axial direction, the sources at corresponding axial locations in each body are of the same strength.

In the two-dimensional case, the image system consists of the displaced sources with corresponding sinks of equal strength at the center line. Since the strengths of the image pairs at any cross-section are the same as that of the original source from the single body solution, the sink cancels this source. Hence the two-dimensional system yields only the displaced line of sources, as previously discussed.

In the three-dimensional case, however, such a simple system does not produce a satisfactory result. There is, in this case, a significant component of flow in the axial direction in addition to the radial flow. It is reasoned, however, that an equivalent line source can be assumed at the body center line which contributes only to the radial flow. This is purely a fictitious flow, but suffices to justify an equivalent two-dimensional flowfield which would generate the source-sink pair described in the image system. Note that the source displacement distance, δ, depends only on the geometric relations and is independent of the two-dimensional source strength.

It follows that an appropriate system for the three-dimensional case can be generated by retaining the sources along the center line of the two bodies (isolated solution) and adding an image system consisting of source-sink pairs in each body which are located according to the two-dimensional displacement distances.

The total velocity potential for this two-body system can now be expressed as before and for a body formed by N sources, the potential at a point j is

$$\phi_j=-\sum_{i=1}^{N}\frac{m_i}{4\pi}\left(\frac{1}{\rho_{ij1}}+\frac{1}{\rho_{ij2}}\right)-\sum_{i=1}^{N}\frac{m_i'}{4\pi}\left[\left(\frac{1}{\rho'_{ij1}}+\frac{1}{\rho'_{ij2}}\right)-\left(\frac{1}{\rho_{ij1}}+\frac{1}{\rho_{ij2}}\right)\right] \tag{16}$$

The ρ distances are as illustrated in Fig. 4 and may be expressed as

$$\rho'_{ij1}=[(\delta_i-r_j\sin\theta)^2+(x_j-x_i)^2+(r_j\cos\theta)^2]^{1/2} \tag{17}$$

$$\rho'_{ij2}=[(y_o-\delta_i-r_j\sin\theta)^2+(x_j-x_i)^2+(r_j\cos\theta)^2]^{1/2} \tag{18}$$

$$\rho_{ij1}=[(x_j-x_i)^2+r_j^2]^{1/2} \tag{19}$$

$$\rho_{ij2}=[(y_o-r_j\sin\theta)^2+(x_j-x_i)^2+(r_j\cos\theta)^2]^{1/2} \tag{20}$$

Using Eqs. (4) and (5), and the relation

$$u_\theta=\frac{1}{r}\frac{\partial\phi}{\partial\theta} \tag{21}$$

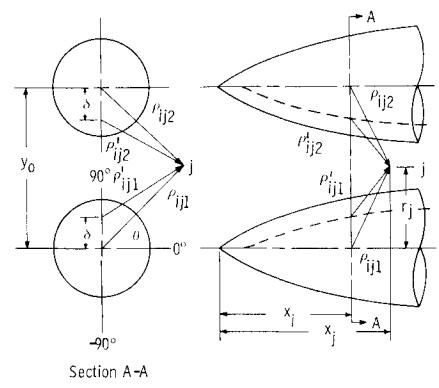

Fig. 4 Geometric relations for the two-body case.

for the velocity components and Eq. (7) for z_i, one may obtain the velocity ratios

$$\frac{u_{x_j}}{U_\infty} = -\sum_{i=1}^{N} [z_i a_{ij} + z'_i (a'_{ij} - a_{ij})] \quad (22)$$

$$\frac{u_{r_j}}{U_\infty} = -\sum_{i=1}^{N} [z_i b_{ij} + z'_i (b'_{ij} - b_{ij})] \quad (23)$$

$$\frac{u_{\theta_j}}{U_\infty} = -\frac{1}{r_j}\sum_{i=1}^{N} [z_i d_{ij} + z'_i (d'_{ij} - d_{ij})] \quad (24)$$

where

$$a_{ij} = \frac{\partial}{\partial x_j}\left(\frac{1}{\rho_{ij1}} + \frac{1}{\rho_{ij2}}\right) \quad (25)$$

$$b_{ij} = \frac{\partial}{\partial r_j}\left(\frac{1}{\rho_{ij1}} + \frac{1}{\rho_{ij2}}\right) \quad (26)$$

$$d_{ij} = \frac{\partial}{\partial \theta_j}\left(\frac{1}{\rho_{ij1}} + \frac{1}{\rho_{ij2}}\right) \quad (27)$$

The terms a'_{ij}, b'_{ij}, and d'_{ij} are formed from Eqs. (25-27) with the values for ρ_{ijk} replaced with the primed quantities; [see Fig. 4, and Eqs. (17-20)]. The unprimed values of z correspond to the single body source strengths, and the primed values represent those of the image system.

The source distribution to correct for the interference is developed by application of the requirement of tangential flow at the body. Using Eqs. (22) and (23) for the velocity components and Eq. (2) for the boundary condition, one may obtain the result

$$\frac{dr_j}{dx_j} - \sum_{i=1}^{N} z_i\left(a_{ij}\frac{dr_j}{dx_j} - b_{ij}\right) = \sum_{i=1}^{N} z_i'\left[a'_{ij}\frac{dr_j}{dx_j} - b'_{ij}\right) - \left(a_{ij}\frac{dr_j}{dx_j} - b_{ij}\right)] \quad (28)$$

Eq. (28) represents a set of N simultaneous equations for determining the source distribution required to account for the interference between two similar bodies. By defining the coefficients of z_i and z'_i as e_{ij} and f_{ij}, respectively, Eq. (28) can be written in the equivalent matrix form

$$\left\{\frac{dr}{dx}\right\} = [e]\{Z\} + [f]\{Z'\} \quad (29)$$

Solving this equation for $\{Z'\}$, one obtains

$$\{Z'\} = [f]^{-1}\left[\left\{\frac{dr}{dx}\right\} - [e]\{Z\}\right] \quad (30)$$

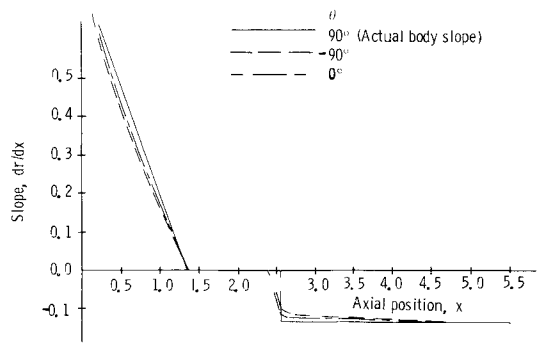

Fig. 5 Comparison of body slope with computed streamlines at meridional angles θ = -90°,0° and 90°.

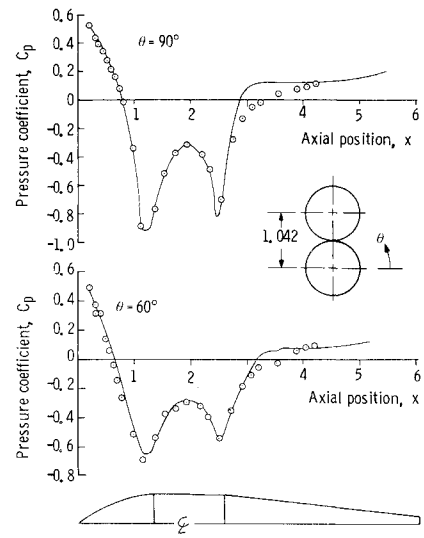

Fig. 6 Comparison of theory and experiment for two-body interference.

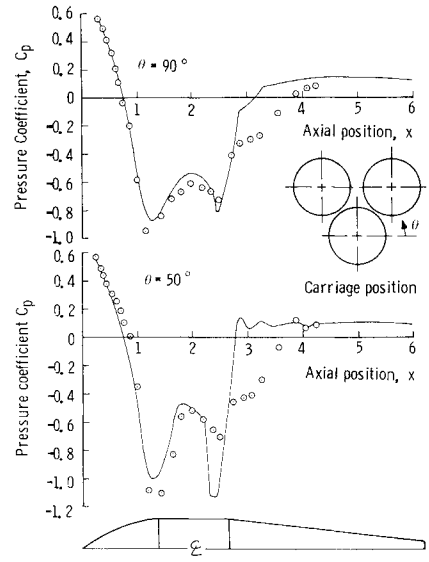

Fig. 7 Comparison of theory and experiment for three-body mutual interference (first-order terms).

The source distribution given by Eq. (30) will satisfy the body boundary condition at N control points and gives good agreement with all other points around the body. It was found that the best location for the control points lie along the intersection of one body with the plane which passes through the center lines of both bodies; i.e., from Fig. 4, the 90° meridional plane. The predicted slopes at other meridional planes are shown on Fig. 5 for an M-117 bomb body shape.

Results for Body-Body Cases

The mutual interference between bodies for the two-, three- and four-body cases have been investigated. However, only the two-body case has the complete image system; the three- and four-body image systems (first-order system) on the third body, etc. The additional source-sink pairs required for the complete n-body image system can be found by repeated application of the Milne-Thomson Circle theorem. Upon investigating the three-body case, however, it was found that the interacting image system found in the next iteration (second-order system) was at most an order of magnitude less important than the first order system.

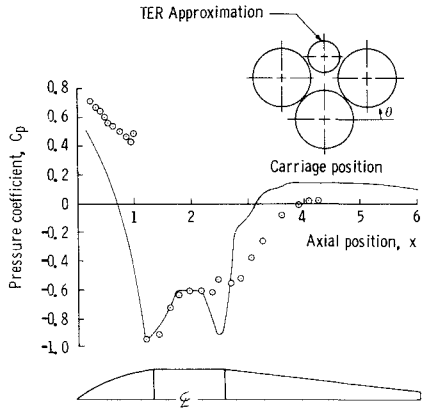

Fig. 8 Comparison of theory and experiment for four-body mutual interference for $\theta = 90°$ (first-order terms only).

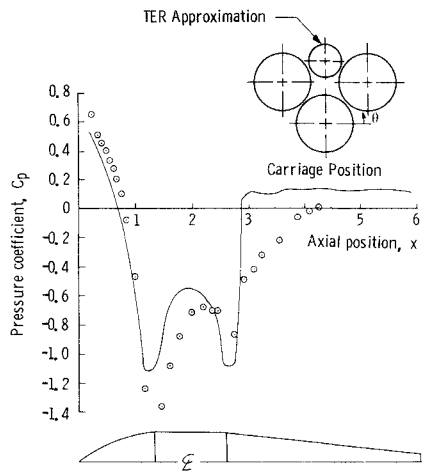

Fig. 9 Comparison of theory and experiment for four-body mutual interference for $\theta = 50°$ (first-order terms only).

The results for the two-body case for a center line displacement of 1.042 body diameters is shown on Fig. 6. This is typical of the agreement between theory and experiment for all meridional angles.

The three-body interference problem was investigated using three M-117 bomb shapes spaced as if mounted on a TER with the active model at Station 1. The agreement between the theory and experiment is shown in Fig. 7.

The four-body problem; TER and three M-117 bombs; was tested and compared with the theoretical results where the TER is approximated as an equivalent body of revolution (not a good approximation because of the bomb racks). This result is shown in Fig. 8 and 9.

As can be seen from Fig. 7-9, there is good agreement between theory and experiment. However, there is evidence of a separation on the boat tail for the three- and four-body cases. This region of separation must be predicted and accounted for if the potential flow solution is to give good agreement along the boat tail.

The agreement between the theoretical and experimental results shows the validity of the analytical approach. it is felt that this approach to the interference problem is a significant advancement in that this technique requires only successive superposition whereas most other methods such as vortex lattice, source panels, etc., require, in general, simultaneous solutions.

References

[1] Woodward, F. A., "Analysis and Design of Wing-Body Combinations at Subsonic and Supersonic Speeds," *Journal of Aircraft*, Vol. 5, Nov.-Dec. 1968, pp. 528-534.

[2] Bradley, R. G. and Miller, R. D., "Application of Finite-Element Theory to Airplane Configurations," *Journal of Aircraft*, Vol. 8, June 1971, pp. 400-405.

[3] Kalman, T. P., Rodden, W. P., and Giesing, J. P., "Application of the Doublet-Lattice Method to Nonplanar Configurations in Subsonic Flow," *Journal of Aircraft*, Vol. 8, June 1971, pp. 406-413.

[4] Smith, C. J., "Mutual Aerodynamic Interference Effects for Two Similar Bodies," M.S. thesis, Aerospace Engineering Department, Auburn University, Auburn, Ala., Dec. 1972.

[5] Walkley, K. B., "Aerodynamic Interference of Wing-Pylon-Body Combinations at Low Subsonic Speeds," M.S. thesis, Aerospace Engineering Department, Auburn University, Auburn, Ala., June 1973.

[6] Martin, F. W., "Mutual Aerodynamic Interference Effects by the Cross-Flow Corrections Method," AFATL-TR-71-69, June 1971, Air Force Armament Laboratory, Eglin Air Force Base , Florida.

[7] Martin, F. W., "Cross-Flow Corrected Axisymmetric Solution for Multiple Body Interference," AFATL-TR-71-109, Aug. 1971, Air Force Armament Laboratory, Eglin Air Force Base, Florida.